Vol.10, Issue No 3, Sep 2020

EXAMINING THE RAILWAY CARS' VIBRATION TRANSMISSIBILITY VIA BENDS WITH LATERAL TRACK IRREGULARITIES

Bhaskar.B.Katti, Hafeezgayasudin.K, Dr.B.H.Manjunath

Asst. Prof, Asst. Prof, Prof. & HOD

bbkatti@pdit.ac.in, hafeezbellary@gmail.com, bhmanj@gmail.com

Department of Mech, Proudhadevaraya Institute of Technology, Abheraj Baldota Rd, Indiranagar, Hosapete, Karnataka-583225

Abstract

This paper describes an investigation into the vibration characteristics resulting from lateral track irregularities that are transferred and become lateral vehicle vibrations when a railway car transits a curved section of track. These transfer characteristics are derived via vehicle dynamics simulations that take into consideration nonlinear characteristics such as flange contact between the wheels and rail. The derived results revealed that the transmissibility of wheel-set lateral movement from lateral track irregularity is larger on a curved section of track than that on a straight section due to restrictions between the wheel flange and rail. Consequently, the mechanism of vibration transfer that occurs when a railway vehicle is transiting a curved section of track can be theoretically explained.

Keywords: Vehicle dynamics, Railway, Bogie, Wheel-set, Lateral vibration, Transmissibility

1. Introduction

When designing modern railway vehicles, vehicle dynamics simulations provide an inclusive way to predict and evaluate the vibrations experienced by vehicles running on an assumed section of track. In general, such vehicle vibrations are considered to be caused by the following. Initially, wheel-set vibrations are excited by track inputs such as track irregularities and the alignment of track effects (such as the radius and cant of the curve), after which the excited wheel-set vibrations are transmitted into the vehicle body through the bogie suspensions. Therefore, to achieve the desired vehicle vibration characteristics, it is necessary to clarify the mechanism by which vibrations resulting from lateral track irregularities are transferred into railway vehicles.

In previous studies regarding vehicles traveling on straight sections of rail, a linearized vehicle dynamics model, in which the creep force between the wheel and rail is modeled linearly, has been used to evaluate the vibration transfer characteristics (Fujimoto et al., 1987) (Sasaki, 1991) (Toshimitsu et al., 2007) because the wheel-set displacement relative to track can be assumed to be small. As for vehicles traveling on curved track sections, running safety evaluations aimed at preventing derailment induced by the contact force between the wheel and rail are crucially important. As a result, there have been many studies in which the contact force between vehicle wheels and rails has been evaluated in terms of running safety (Hirotsu et al., 1997) (Hirotsu et al., 1999). For example, a detailed study of vehicle dynamics in which the nonlinear characteristics of the creep force between the wheels and rails were modeled was previously reported (Hirotsu et al., 1999).

In contrast, there have been few studies that examined the mechanisms and characteristics of vibration transfers resulting from lateral track irregularities into vehicle responses on curved track sections. In this study, the vehicle dynamics model constructed and used in previous studies (Hirotsu et al., 1999) (Hidai et al., 2014) is used for the mechanism clarification. The novelty of this study is that the differences in vibration transfer characteristics between straight and curved sections of track, as well as the mechanisms of those differences, have been clarified.

The remainder of this paper is organized as follows. In Section 2, the calculation conditions are described. In Section 3, vehicle dynamics simulations are carried out on both curved and straight track sections that were artificially generated

to replicate actual railway conditions and which possess the same lateral track irregularities. Then, the differences in lateral vehicle vibrations between the straight and curved sections are clarified. In Section 4, vehicle dynamics simulations are carried out on both curved and straight sections without lateral track irregularities, and the differences in the wheel-rail contact position at curved and straight sections are clarified. In Section 5, vehicle dynamics simulations are carried out on both curved and straight sections with sine-wave lateral track irregularities, from which the differences in lateral vibration transmissibility from the track to the vehicle that result from track irregularities are clarified.

2. Calculation conditions

2.1 Vehicle dynamics model

Figure 1 shows a one-vehicle dynamics simulation model. This model, which consists of seven rigid bodies (one vehicle body, two bogies, and four wheel-sets), has 43 degrees of freedom. Each rigid body in the vehicle model is characterized by its mass, its inertia, and the geometric position of its center of gravity. Furthermore, each rigid body (except for the vehicle body) has six degrees of freedom expressing its motions in the longitudinal, lateral, vertical, roll, pitch, and yaw directions. The vehicle body has seven degrees of freedom because it is divided into front and rear sections in order to consider its torsional stiffness. Each rigid body is connected by suspension elements such as the stiffness and damping. The wheel-rail contact forces are determined in accordance with the Levi-Chartet equation (Kalker, J. J., 1979). The rolling radius and contact angle, which depend on the relative position between the wheel and rail, are also considered. This allows the examination of nonlinear phenomena such as flange contact between the wheel flange and rail. The coordinate system used in this study is right-handed, located at the position of the center of gravity, and change with vehicle moving. The detailed equation of motion for the vehicle model, in which generic high-speed train parameters with an inter-car damper are used, was described in these papers. (Hirotsu et al., 1999) (Hidai et al., 2014.) The actual parameters described in these papers (Tanifuji et al., 2006) (Toshimitsu et al., 2007) are used in this study as well. The train model, which was made by connecting five vehicle models, is the same as that used in the paper (Hidai et al., 2014). The knowledge related to the vibration transfer mechanism on a curved section of track described in this study can be obtained via the one vehicle model.

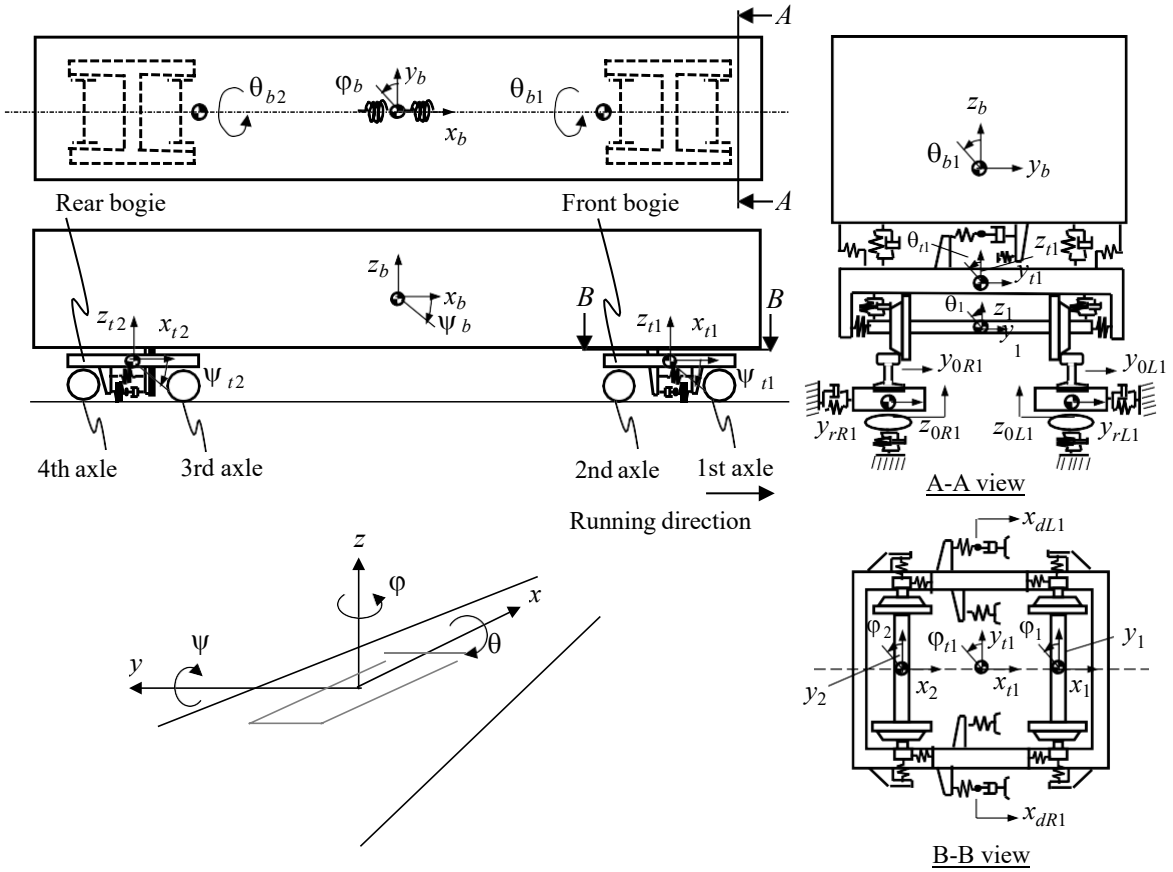

Fig. 1 Vehicle dynamics model

2.2 Track geometry and running speed

Table 1 shows the track geometry conditions. In the three cases shown in this table, the track irregularity and velocity are exactly the same; only the track geometry is different. In Cases 1 and 2, in order to equalize the centrifugal acceleration acting on the vehicle in each case, the curve radius and cant are designated. Figures 2 and 3 show the curvature and cant geometries used for the numerical simulation. The track irregularity conditions are described in Section 2.3.

Table 1 Track geometry and running speed

		Case 1	Case 2	Case 3
(i)	Curve radius [m]	2000	5000	Straight
	Cant [mm]	200	12.5	0
(ii)	Velocity [km/h]	230	230	230
(iii)	Track irregularity	Artificially generated	←	←

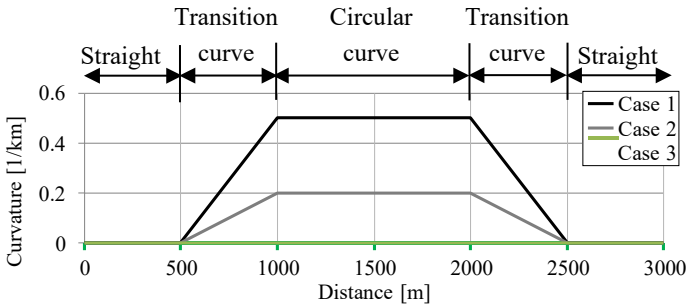

Fig. 2 Track curvature for vehicle dynamics simulation

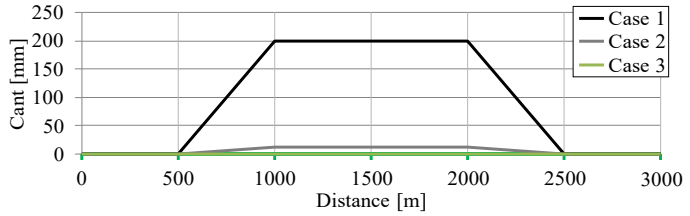

Fig. 3 Cant for vehicle dynamics simulation

2.3 Lateral track irregularity

Lateral track irregularity conditions are defined from Section 3 to 5 as follows:

Section 3: To clarify the lateral vehicle vibration differences between the curved and straight track sections, vehicle dynamics simulations are carried out with the same lateral track irregularity for both section types. This lateral track irregularity is artificially generated by an inverse Fourier transform from the generic track power spectrum density (Tanifuji et al., 1990). Figure 4 shows the normalized track irregularity transient input. In this paper, the time histories for both track irregularity and wheel-set lateral displacement are normalized by the nominal gap between the wheel flange and rail.

Section 4: To clarify the difference in the wheel-rail contact position between the curved and straight track sections, vehicle dynamics simulations are carried out without lateral track irregularity for both section types.

Section 5: To clarify the difference in transmissibility characteristics between curved and straight track sections, vehicle dynamics simulations are carried out with sine-wave lateral track irregularity for both section types.

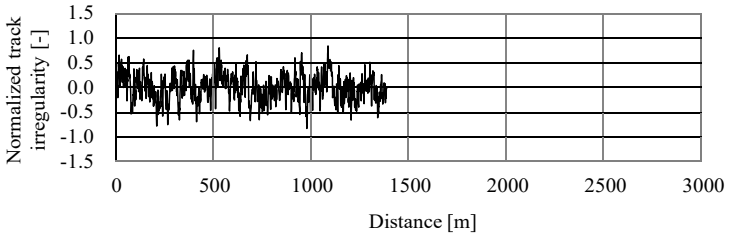

Fig. 4 Transient input of normalized lateral track irregularity for vehicle dynamics simulation

3. Lateral vehicle vibration comparison between straight and curved cases with lateral track irregularity

Figure 5 shows the time history of normalized car-body lateral acceleration in which the acceleration is normalized by a certain steady condition. From this figure, the time histories for three cases are compared. (i) In the straight sections (0 to 500 m and 2500 to 3000 m), each time history is almost the same because the track geometry conditions, velocity, and track irregularity are completely the same. In contrast, (ii) in the curved section (500 to 2500 m), especially in the circular curve area (1000 to 2000 m), even though the same lateral track irregularity is applied to the vehicle, there are differences in the amplitude of the car-body lateral acceleration. Specifically, as the curve radius decreases, the amplitude of the car-body lateral acceleration increases. Next, the frequency response of the car-body lateral acceleration will be investigated.

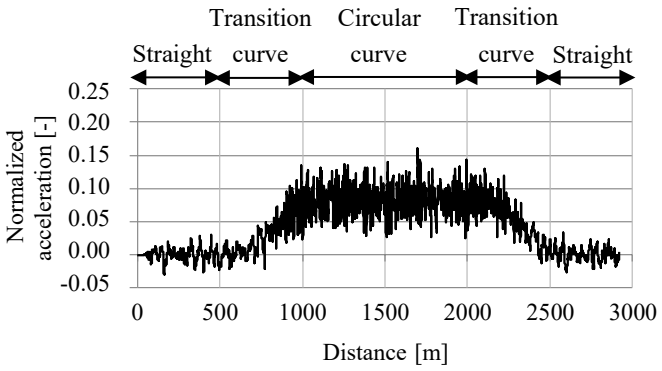

(a) Case 1, 2000 m curve radius

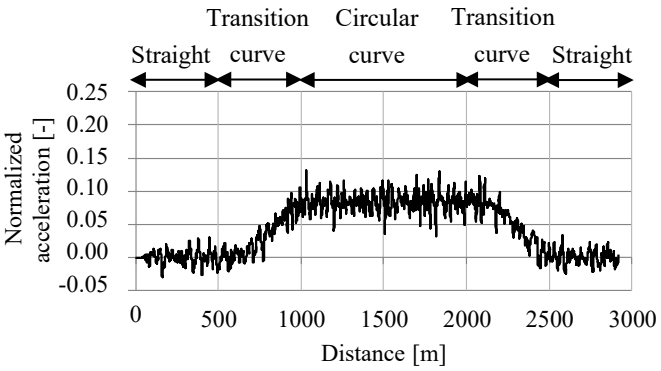

(b) Case 2, 5000 m curve radius

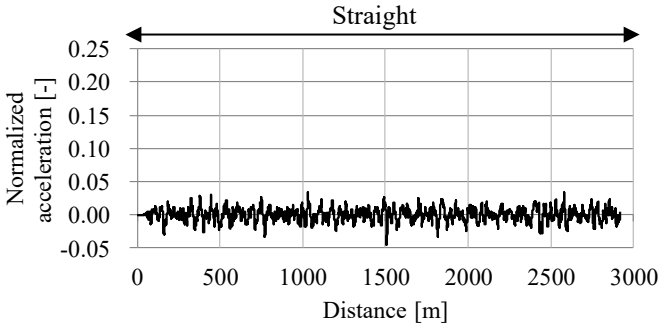

(c) Case 3, Straight section

Fig. 5 Time histories of normalized car-body lateral acceleration at the car-body floor above the front bogie. Despite applying the same lateral track irregularity, the amplitude of lateral car-body acceleration among the curved track cases and straight track case is different in the section of 500 to 2500m.

Figure 6 shows the power spectrum density converted from the entire time histories in Fig. 5. First, in the frequency range under 0.5 Hz shown in (a), it can be seen that the frequency responses for the curved cases are larger than that for the straight track case and that both curved cases have almost the same frequency responses. Second, in the frequency range from 0.5 to 2 Hz shown in (b), the frequency responses for the curved cases are smaller than that for the straight track case, and the frequency response for the 2000 m curved radius is smaller than that for the 5000 m curved radius.

Third, in the frequency range over 2 Hz shown in (c), the frequency responses for the curved cases are larger than that for the straight track case, and the frequency response for the 2000 m curved radius is larger than that for the 5000 m curved radius.

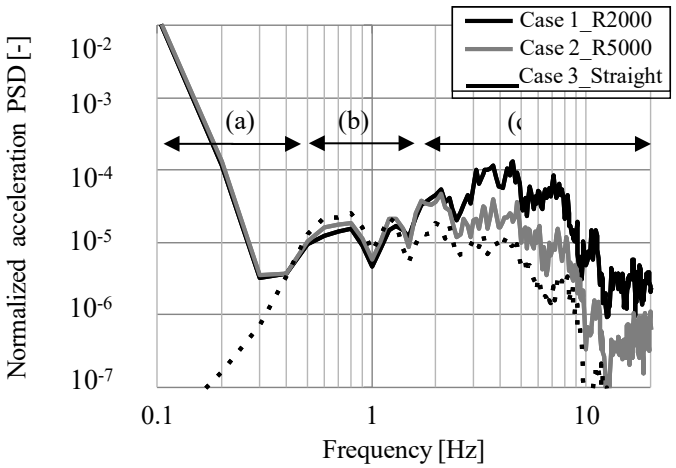

Fig. 6 Normalized power spectrum density of car-body lateral acceleration at the car-body floor above the front bogie. The magnitude relationship of the power spectrum density among the curved track cases and the straight track case changes at the boundary of around 2Hz.

Next, the difference in the power spectrum density for each case is described. For the frequency range below 0.5 Hz shown in (a), the frequency response difference is considered to be due to the influence of the centrifugal acceleration transient response generated through the curved section.

For the frequency range over 0.5 Hz, as shown in (b) and (c), these frequency response differences are considered to be due to the difference in wheel and rail contact conditions. This is because the only difference between each case is that the vehicle is excited by a lateral track irregularity under different wheel and rail contact conditions. Accordingly, the wheel and rail contact position differences will be clarified in Section 4.

4. Wheel-rail contact position comparison between straight and curve cases

Figure 7 shows the time history of the normalized lateral displacement of the first wheel-set without lateral track irregularity. Here, the displacement is normalized by the nominal gap between the wheel flange and the rail. A positive value means that the wheel-set moves to the outside of the curve. In this figure, it can be seen that the wheel-set lateral displacement for the 2000 m curve radius is larger than that for the 5000 m curve radius. This means that the wheel-rail contact position for the 2000 m curve radius is closer to the flange position than that for the 5000 m curve radius. Figure 8 summarizes the steady values of normalized wheel-set lateral displacement for all wheel-sets. The flange contact position in this figure is shown by a horizontal line.

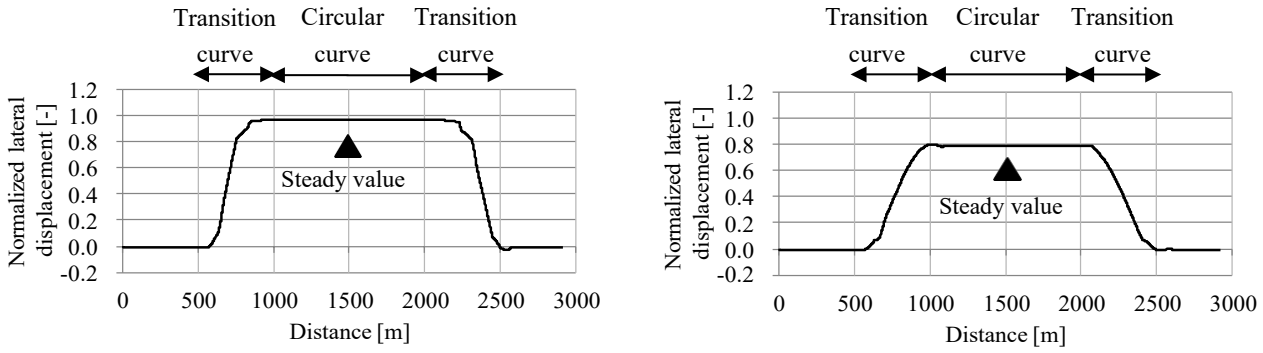

(a) Case 1, 2000 m curve radius (b) Case 2, 5000 m curve radius

Fig. 7 Time histories of normalized first wheel-set lateral displacement

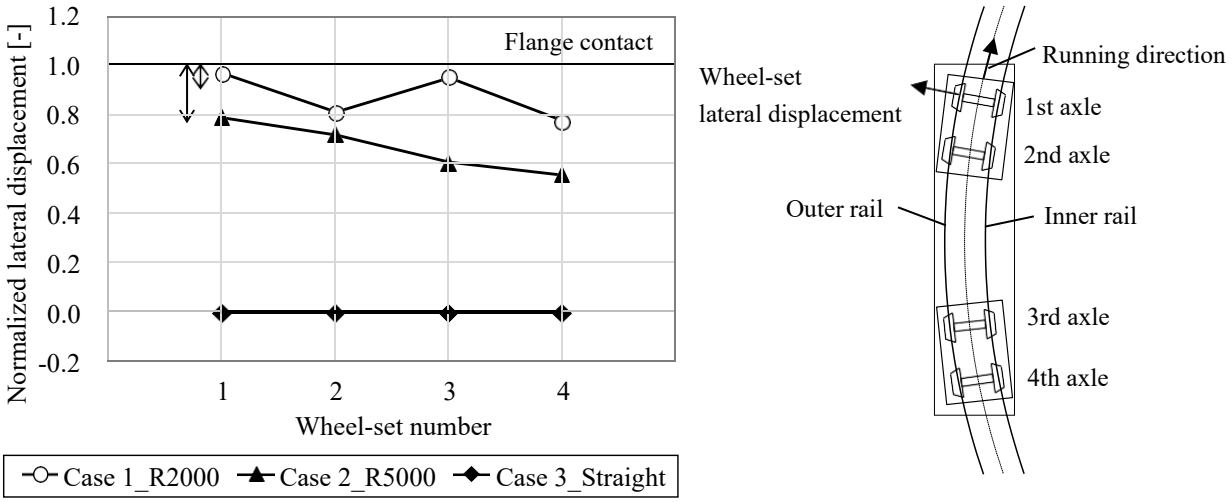

Fig. 8 Normalized wheel-set lateral steady displacement for curved and straight cases. As the curve radius decreases, the gap between the wheel flange and the rail decreases.

In Fig. 8, if the steady value plot is smaller than 1.0, there is a gap between the wheel flange and the rail. In the straight track section case, the steady values of all wheel-sets are plotted at zero because no wheel-sets move in the straight section that do not have track irregularity. Figure 8 also shows that the gap between the wheel flange and the rail for the curved track cases is smaller than that for the straight track case. Furthermore, as the curve radius decreases, the gap between the wheel flange and the rail decreases as well. This is because the wheel-set needs to move outward in the curved section in order to secure the rolling radius difference.

5. Vibration transmissibility comparison between straight and curve cases

5.1 Procedure

In this section, in order to examine the mechanism causing the lateral vehicle vibration differences between the straight and curved track sections during the assumed actual lateral track irregularity, which is shown in Fig. 6, we investigate the vibration transmissibility and wheel-set behavior by applying a sine-wave lateral track irregularity as a basic input for each frequency. The transmissibility is then evaluated by the following procedure.

First, a vehicle dynamics simulation is carried out to obtain the relationship between the "Input," which means the lateral track irregularity, and the "Output," which means the lateral vehicle vibration. Here, the sine-wave lateral track irregularity is used. The response of each part of the vehicle exhibits mostly sine-wave characteristics.

Second, the vibration transmissibility is defined from Eqs. (1) to (3) by calculating the amplitude ratio between the Input and Output. Here, the frequency cases of sine-wave input from 0.2 to 2 Hz are evaluated in 0.2 Hz steps, and those from 2 to 10 Hz are evaluated in 0.5 Hz steps. In Eqs. (1) to (3), the total displacement between peak of upper side and peak of lower side is defined as the amplitude. The amplitude of the sine-wave lateral track irregularity was set to 0.75 with reference to the root-mean-square (RMS) value of the assumed lateral track irregularity shown in Fig. 4. For the amplitude dependence, it was confirmed that the results obtained in this study do not change even if the amplitude is set smaller than the value defined above.

$$G_{wheel-set\_dis} = D_{wheel-set}/w_{input} \quad (1)$$

$$G_{bogie\_acc} = {}_{bogie}/w_{input} \quad (2)$$

$$G_{car-body\_acc} = {}_{car-body}/w_{input} \quad (3)$$

Where:

$G_{wheel-set\_disp}$: Vibration transmissibility of wheel-set lateral displacement
G_{bogie_acc} : Vibration transmissibility of bogie lateral acceleration
$G_{car-body\_acc}$: Vibration transmissibility of car-body lateral acceleration

w_{input} : Amplitude of sine-wave lateral track irregularity
$D_{wheel-set}$: Amplitude of wheel-set lateral displacement
A_{bogie} : Amplitude of bogie lateral acceleration
$A_{car-body}$: Amplitude of car-body lateral acceleration

5.2 Simulation results for vibration transmissibility for wheel-set lateral displacement

Figure 9 shows the time history examples used for the lateral displacement of the first wheel-set with a sine-wave lateral track irregularity in order to derive the vibration transmissibility. The transmissibility can be calculated by Eq. (1). In Fig. 9, the calculated transmissibility values with the two curved cases and one straight case are shown. The simulation results for the excited frequency of 1 and 2 Hz are shown as representative cases. For other frequency cases, the vibration transmissibility for each case is evaluated in the same manner as shown here. The entire simulation results are as shown below.

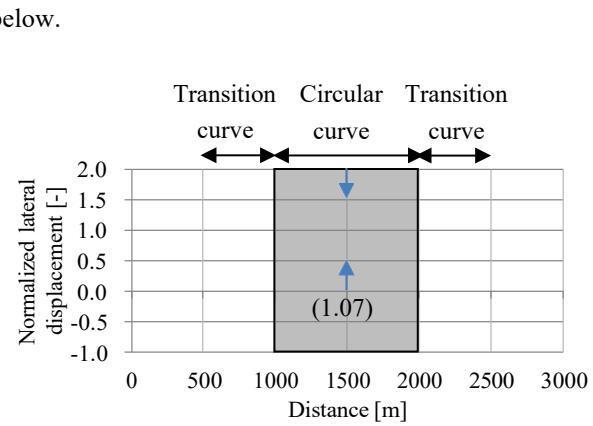

(a) Case 1, 2000 m curve radius

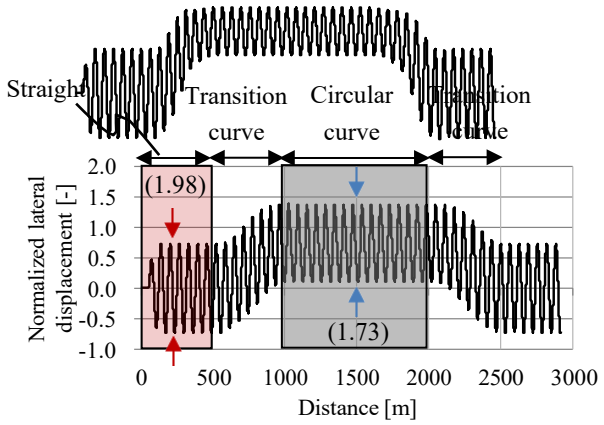

(b) Case 2, 5000 m curve radius

(i) 1 Hz sine-wave track input

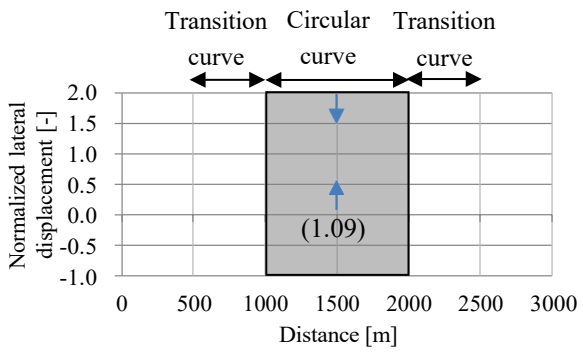

(a) Case 1, 2000 m curve radius

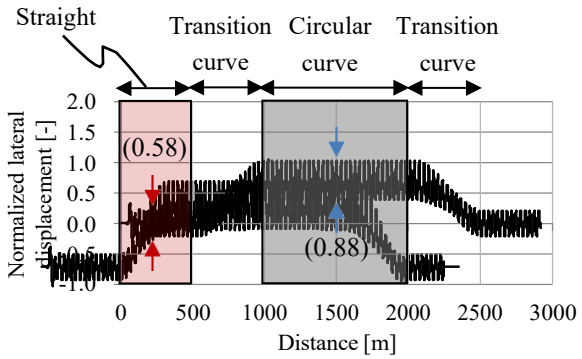

(b) Case 2, 5000 m curve radius

(ii) 2 Hz sine-wave track input

Fig. 9 Time histories of normalized first wheel-set lateral displacement with sine-wave track input

Figure 10 shows the vibration transmissibility response of wheel-set lateral displacement for a sine-wave lateral track irregularity in the range from 0.2 to 10 Hz. As can be seen in the figure, for the straight case (Case 3), the transmissibility response clearly peaks around 1 Hz and tends to decrease over 1 Hz. In the more tightly curved case (Case 1), the transmissibility response is maintained at around 1.0 in the range from 0.2 to 4 Hz.

The relationship of transmissibility between the straight and curved cases is as follows: (i) In the frequency range from 0.5 to 2 Hz, the transmissibility for the straight case is larger than those for the curved cases. (ii) In the frequency range over 2 Hz, the transmissibility for the curved cases are larger than that for the straight case. Next, the mechanism investigation for the straight and curved cases is clarified in Sections 5.3 and 5.4.

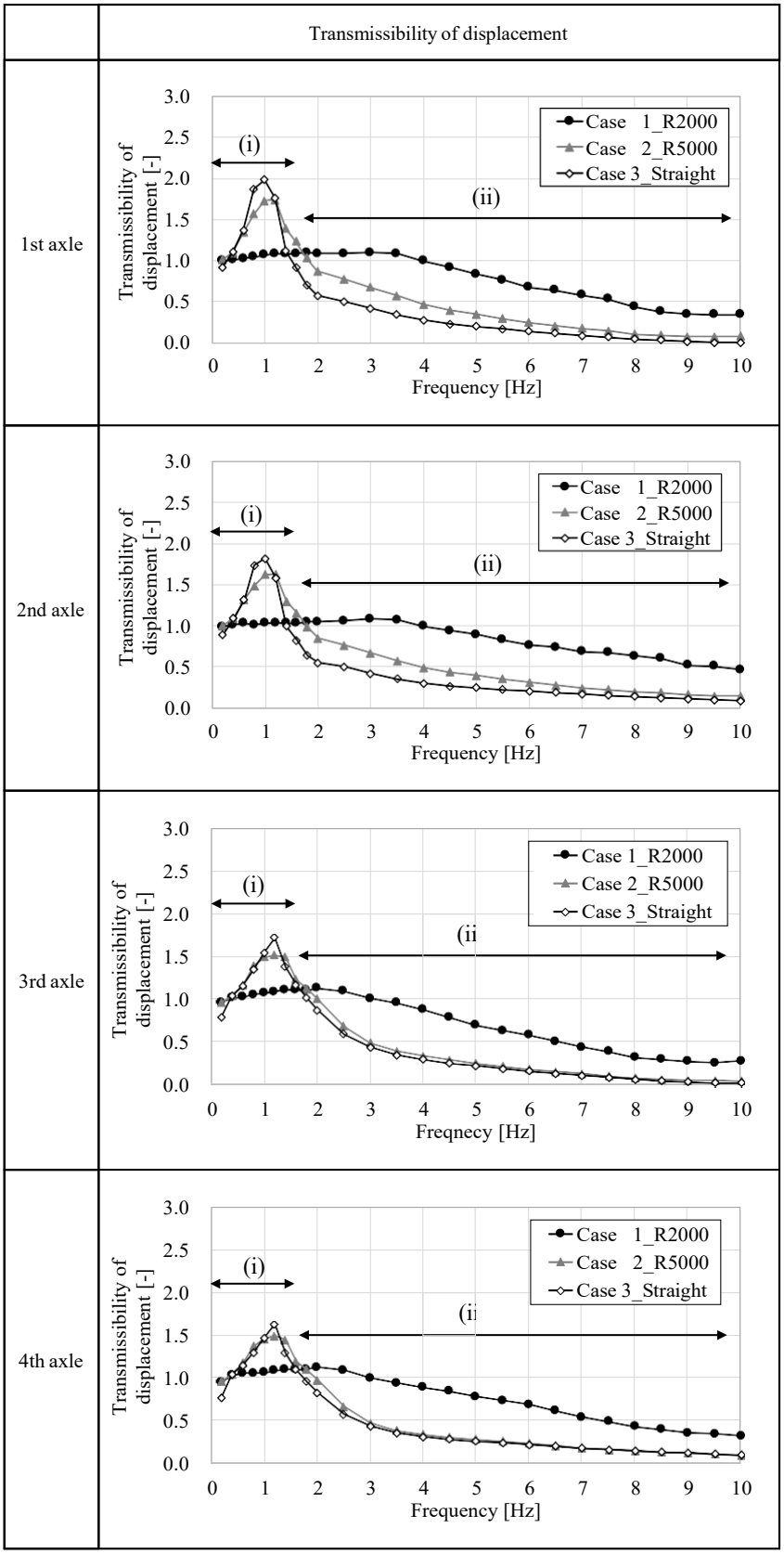

Fig. 10 Transmissibility of wheel-set lateral displacement from the sine-wave track input. The magnitude relationship of transmissibility among the curved track cases and the straight track case changes at the boundary of 2Hz.

5.3 Mechanism investigation for the straight case

The transmissibility peak phenomena around 1 Hz for the straight section case is investigated by a single-bogie model, as shown in Fig. 11. The motivation for conducting the examination by the single-bogie model is described below.For the full vehicle model used in this paper, the natural frequency of the vehicle's rigid body vibration modes (such as the sway and yaw mode) exists around 1 Hz. Therefore, it is necessary to clarify whether or not the bogie also has a vibration mode around 1 Hz. Accordingly, this model consists of a bogie frame, two wheel-sets, primary suspension, and secondary suspension. The end of each secondary suspension is fixed to the ground. The fundamental equations are shown from Eqs. (4) to (11). In Eqs. (6) and (7), it can be seen that the equivalent conicity is 1/20, and the other parameters are the same as those used in the full vehicle model.

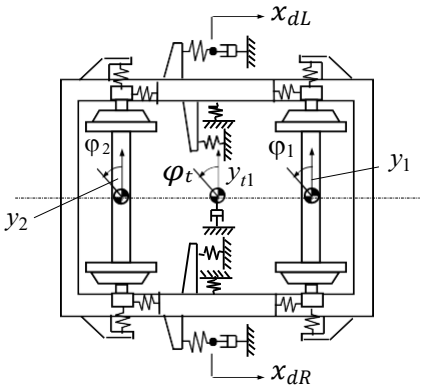

Fig. 11 Single-bogie model

$$m_w\ddot{y}_1 = 2k_w(y_t + a\varphi_t - y_1) - 2f_2\dot{y}_1/V + 2f_2\varphi_1 \quad (4)$$

$$m_w\ddot{y}_1 = 2k_w(y_t + a\varphi_t - y_1) - 2f_2\dot{y}_1/V + 2f_2\varphi_1 \quad (5)$$

$$J_w\ddot{\varphi}_1 = 2k_{wx}b_1^2(\varphi_t - \varphi_1) - 2f_1b_0^2\dot{\varphi}_1/V - 2b_0f_1\gamma(y_1 - w_1)/r_0 \quad (6)$$

$$J_w\ddot{\varphi}_2 = 2k_{wx}b_1^2(\varphi_t - \varphi_2) - 2f_1b_0^2\dot{\varphi}_2/V - 2b_0f_1\gamma(y_2 - w_2)/r_0 \quad (7)$$

$$m_t\ddot{y}_t = -2k_{wy}(y_t + a\varphi_t - y_1) - 2k_w(y_t - a\varphi_t - y_2) - 2k_{2y}y_{t1} - c_{2y}\dot{y}_{t1} \quad (8)$$

$$J_t\ddot{\varphi}_t = -2k_{wx}b_1^2(\varphi_t - \varphi_1) - 2k_{wx}b_1^2(\varphi_t - \varphi_2) - 2k_{2x}b_2^2\varphi_t$$
$$-k_{yaw}b_3(b_3\varphi_t - x_{dR}) - k_{yaw}b_3(b_3\varphi_t + x_{dL}) \quad (9)$$

$$k_{ya}(b_3\varphi_t - x_{dR}) - c_{yaw}\dot{x}_{dR} = 0 \quad (10)$$

$$k_{ya}(-b_3\varphi_t - x_{dL}) - c_{yaw}\dot{x}_{dL} = 0 \quad (11)$$

In the equation of motion shown above, the lateral track irregularity (w_1, w_2) is defined as the input signal, while the wheel-set lateral displacement (y_1) is defined as the output signal. Thus, the state-space system for a single-bogie model can be derived from the equation of motion as two inputs (w_1, w_2) and one output (y_1). Since the lateral track irregularity of the second axle (w_2) can be expressed by multiplying the time-delay function by the lateral track irregularity of the first axle (w_1), the single-bogie model can be expressed as a single-input single-output (SISO) system (Tanifuji et al., 2000), while the vibration transmissibility from the lateral track irregularity (1) to the first wheel-set lateral displacement (y_1) can be derived as a transfer function.

Figure 12 shows the transmissibility response calculated by the single-bogie model. In the same figure, the transmissibility response for the first wheel-set lateral displacement calculated using the full vehicle model is also plotted for comparison. Here, the transmissibility response for a single-bogie model can be shown as a continuous line because it is a linear system model. In contrast, the transmissibility response for a full vehicle model can be obtained as a discrete plot because the response was obtained for each frequency, as described in Section 5.1.

From Fig. 12, we can see that the single-bogie model exhibits a transmissibility peak at around 1 Hz. This peak shows resonance phenomena in the bogie hunting mode, in which the amplitude and phase of lateral and yaw movements are almost the same for the bogie-frame, first wheel-set, and second wheel-set. The transmissibility response declines after exceeding the resonance frequency. The simulation result trend is consistent with a study in which a single-bogie model was used to analyze the transmissibility response (Guandong, 2017). It can also be seen that the peak magnitude around 1 Hz obtained with the single-bogie model is smaller than that obtained with the full vehicle model. This occurs because

the damping ratio for the bogie hunting mode with a single-bogie model becomes larger than that with the full vehicle model due to the fact that the end of each secondary suspension is fixed to the ground, where the displacement is completely restricted.

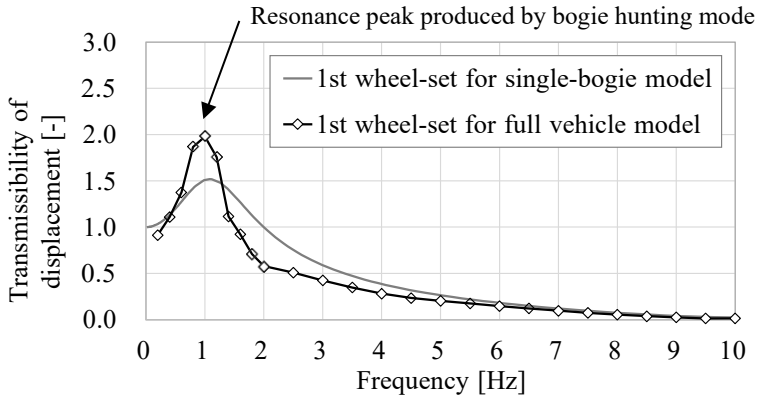

Fig. 12 Comparison of vibration transmissibility for first wheel-set lateral displacement resulting from a lateral track irregularity between the single bogie and full vehicle models. Single-bogie has a resonance peak at around 1Hz by the bogie hunting mode. This result indicates that bogie has a vibration mode around 1Hz when the bogie parameters designated in this paper are used.

From the above examination, it was found that the single-bogie model has a bogie hunting mode around 1 Hz when the bogie parameters and velocity of 230 km/h designated in this report are used. We also found that the amplitude of the wheel-set lateral displacement becomes larger than the lateral track irregularity amplitude due to the resonance phenomena produced by the bogie hunting mode. Furthermore, since the frequency of the bogie hunting mode and the frequency of vehicle sway and yaw mode are close to each other, it is considered likely that the frequency response of the lateral vehicle acceleration has a peak around 1 Hz, as shown in Fig. 6. This finding is similar to that reported in a previous study (Fujimoto, 1998).

5.4 Mechanism investigation for the curved case

Next, the behavior of a wheel-set with a sine-wave lateral track irregularity traveling on a curved section of track is examined. Figure 13 shows the sine-wave lateral track irregularity and wheel-set lateral displacement time histories for the 1 Hz case as the condition that produces the resonance frequency that was found to exist in the straight track case examined in Section 5.3, while Fig. 14 shows the calculation results for the phase delay in the frequency range under 4 Hz.

First, from Fig. 13, it can be seen that in the case of a straight section where there is sufficient flange clearance (as shown in Fig. 8), the wheel-set lateral displacement amplitude is about twice the amplitude of the track input. This effect results from the resonance phenomena caused by the bogie hunting mode that was explained in Section 5.3.

Second, in the case of the 5000 m curve radius, the wheel-set lateral displacement amplitude tends to increase, but the displacement is restrained by the wheel flange and rail during the displacement amplification process. This effect can be confirmed as a waveform distortion.

Third, in the case of the 2000 m curve radius where there is slight flange clearance, as shown in Fig. 8, the wheel-set lateral displacement amplitude is almost the same as the track input amplitude, and there is almost no phase delay between the wheel-set lateral displacement and the track input, as shown in Fig. 14. In other words, in the case of the 2000 m curve radius, the wheel-set lateral movement is nearly synchronized with the track input due to the wheel and rail flange restriction.

This wheel-set behavior is why the wheel-set lateral displacement vibration transmissibility becomes about 1.0 in the next higher frequency band above the bogie hunting resonance frequency. As a result, the transmissibility response of a wheel-set traveling on a curved section is larger than that found of a wheel-set on a straight section in the next higher frequency band above the bogie hunting resonance frequency.

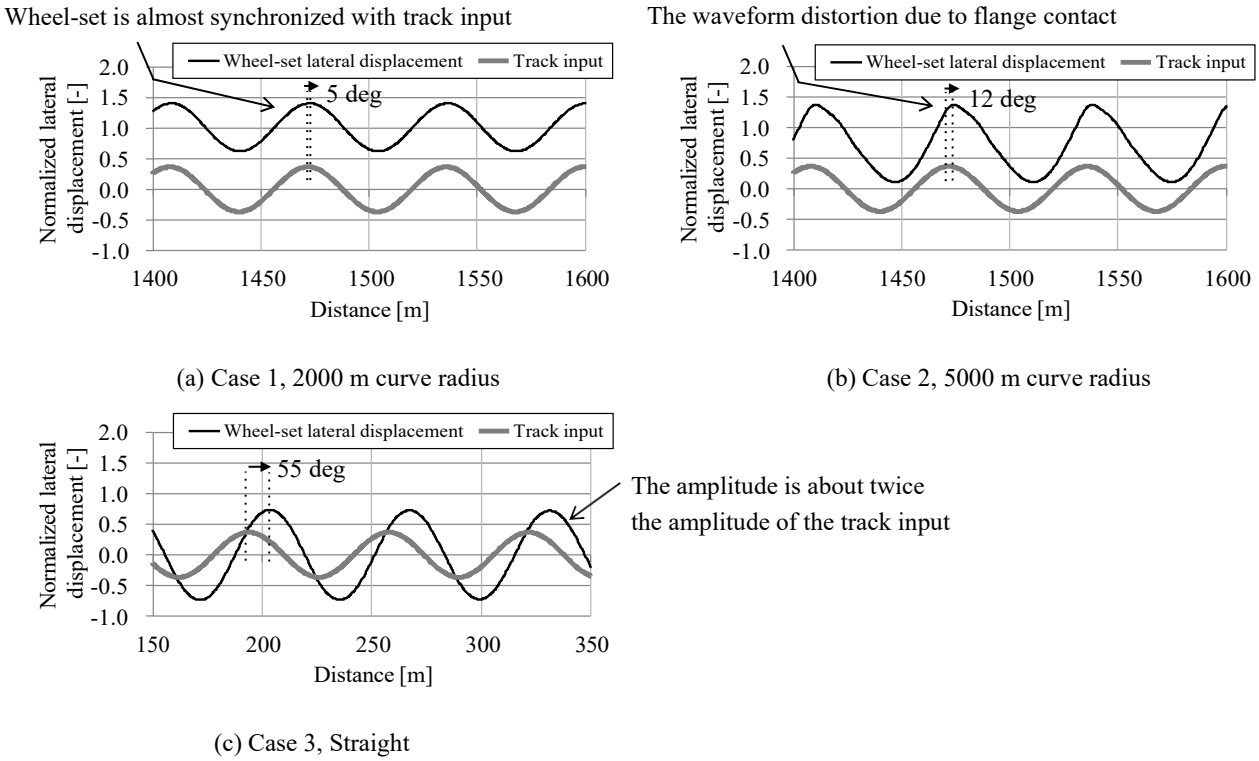

Fig. 13 Time histories of the normalized wheel-set lateral displacement and the sine-wave track input. As the curve radius decreases, the wheel-set is nearly synchronized with the track input due to the restriction between the wheel flange and rail.

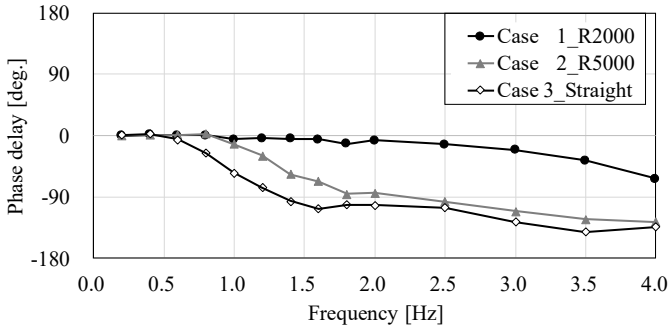

Fig. 14 The phase delay from the track input to the first wheel-set lateral displacement

5.5 Vibration transmissibility of bogie and car-body lateral acceleration

Figure 15 shows the vibration transmissibility response for bogie and car-body lateral acceleration resulting from a sine-wave lateral track irregularity in the range from 0.2 to 10 Hz. The transmissibility relationship between the straight and curved cases is as follows. In the frequency range over 2 Hz, the transmissibility for the curved rail cases are larger than that for the straight rail case. These relationships are the same as the relationship for the wheel-set lateral displacement, as shown in Fig. 10.

Since the suspension parameters are completely the same among all cases, it is considered likely that the magnitude relationship among the curved track cases and the straight track case for car-body and bogie lateral vibration is dominated by the magnitude relationship for the wheel-set lateral vibration, as shown in Fig. 10.

In addition, from Fig. 15 it can be seen that in the case of the 5000 m curve radius, the transmissibility magnitude for the car-body and bogie on the front bogie side is larger than that experienced on the rear bogie side. Additionally, the gap between the wheel flange and rail on the front bogie side is smaller than that on the rear bogie side, as shown in Fig. 8.

Since the wheel-sets on the front side bogie are more influenced by the restriction between the wheel flange and rail,

it is considered likely that the transmissibility response on the front bogie side becomes larger than that experienced on the rear side. As shown above, it can also be understood that the frequency response of transmissibility of wheel-set lateral displacement from lateral track irregularity is an important factor that determines the car-body lateral vibration. Therefore, it can be said that the frequency response design of the wheel-set lateral vibration is an important contributor to the frequency response design of the vehicle's lateral ride comfort.

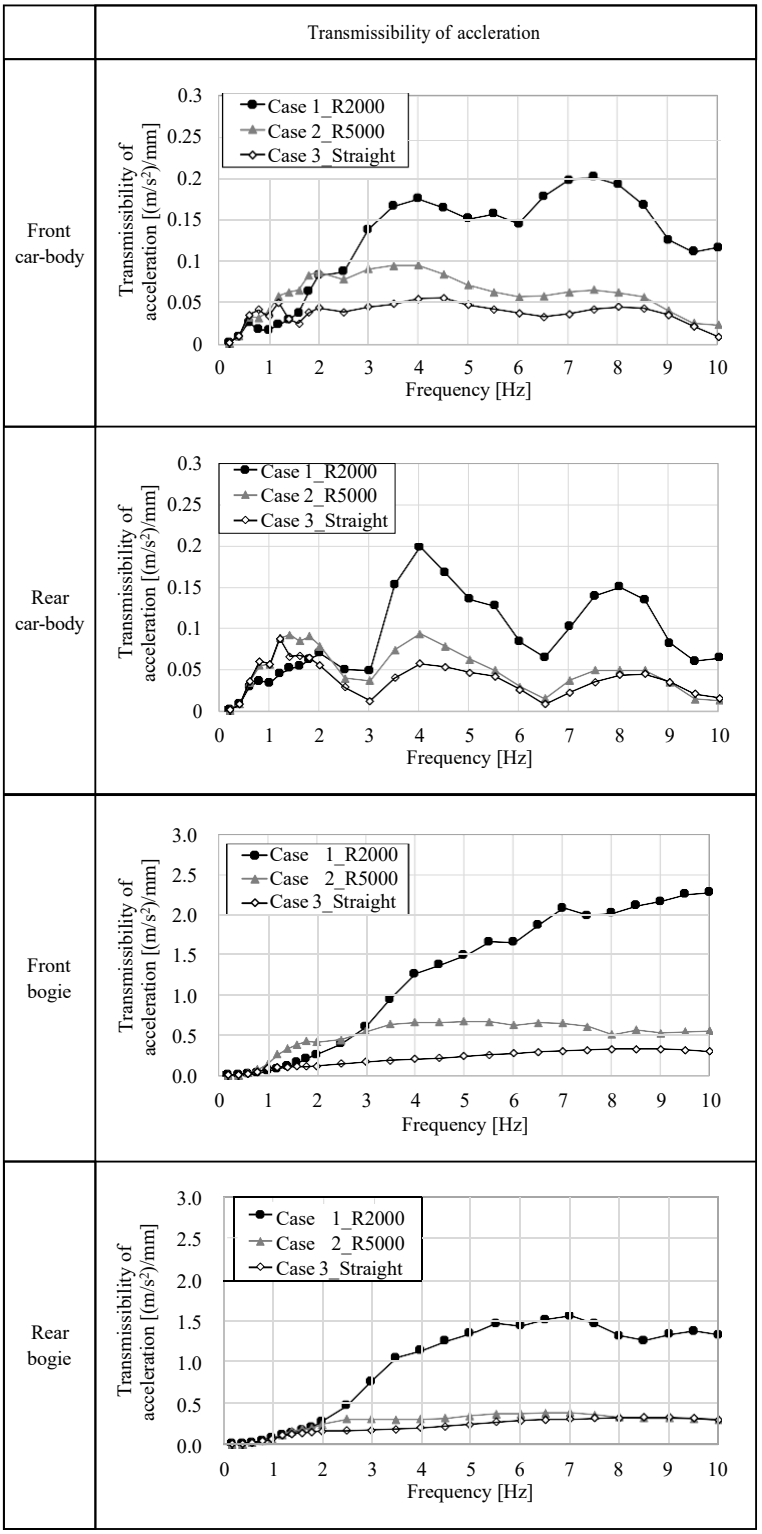

Fig. 15 Transmissibility of car-body and bogie lateral acceleration from the sine-wave input. The magnitude relationship of transmissibility among the curved track cases and the straight track case changes at the boundary of 2Hz. These relationships are the same as the relationships as shown in Fig. 10.

6. Conclusions

This study was an inquiry of how vibration properties caused by lateral track irregularities are transmitted to the lateral vibrations of a train as it travels around a curved length of track.

The transmissibility response of the wheel-set lateral displacement caused by the lateral track irregularity has a resonance peak that is generated by the bogie hunting mode. The response then decreases once it exceeds the resonance frequency, as long as the vehicle is travelling on a straight section of track with a sufficient gap between the wheel flange and rail.

2) In the next higher frequency band above the bogie hunting resonance frequency, the vibration transmissibility response of the wheel-set lateral displacement becomes approximately 1.0 for a vehicle travelling on a curved section of track with a small gap between the wheel flange and the rail. The close proximity of the wheel flange to the rail suggests that the wheel-set is almost in time with the track input.

(3) From (1) and (2), it is clear that beyond the bogie hunting resonance frequency, the vibration transmissibility response of the wheel-set lateral displacement on curved track sections is larger than on straight track sections. Consequently, in the frequency range, the lateral vibration of the car-body is more pronounced on curved parts of track compared to straight ones.

4) The wheel-set transmissibility response and the car-body lateral vibration in the next higher frequency band above the bogie hunting resonance frequency are both affected by the amount of gap between the wheel flange and the rail. The response is stronger as the gap drops.

5) As mentioned earlier, an essential component of the frequency response design needed for the vehicle's lateral ride comfort is the transmissibility of wheel-set lateral displacement from lateral track irregularity.

References

Fujimoto, H., and Miyamoto, M: The vibration of the tail car in a coupled train, Transactions of the Japan Society of Mechanical Engineers(in Japanese), Vol. 53, No. 494 (1987), DOI: 10.1299/kikaic.53.2110

Fujimoto, H: Influence of Arc and Conic Profile on Vehicle Dynamics (An Evaluation from Input Energy and Kinematic Oscillation), Transactions of the Japan Society of Mechanical Engineers (in Japanese), Vol. 64, No. 621 (1998), DOI: 10.1299/kikaic.64.1520

Guandong, L: Advanced Railway Vehicle Dynamics (2017), Section 5

Han, W., Xiao-Hui Z., Jiang L. and Yang Y.: Nonlinear hunting stability of high-speed railway vehicle on a curved track under steady aerodynamic load, Vehicle System Dynamics, Vol. 58, No.32 (2019), DOI: 10.1080/00423114.2019.1572202

Hidai, M., Goda, K., Iwasaki, K., and Watanabe, T: Simulation with curve and aerodynamic force for a coupled railway vehicle, Transactions of the Japan Society of Mechanical Engineers(in Japanese), Vol. 80, No. 813 (2014), DOI: 10.1299/transjsme.2014dr0123

Hirotsu, T., Hiraishi, M., Terada, K., Shimada, M., and Yamada, M: Curving simulation of a pendulum vehicle, Transactions of the Japan Society of Mechanical Engineers (in Japanese), Vol. 63, No. 612 (1997), DOI: 10.1299/kikaic.63.2671

Hirotsu, T., Shimada, M., Nishigaito, T., Miyajima, A. Kakehi, Y., and Muramoto, T: Curving simulation of a non-pendulum rail vehicle, Transactions of the Japan Society of Mechanical Engineers (in Japanese), Vol. 65, No. 637 (1999), DOI: 10.1299/kikaic.65.3531

Kalker, J. J., Vehicle System Dynamics (1979), 8-4

Sasaki, K: Development of Bogies for Improving the Riding Comfort of the Shinkansen (Improved Bogies for the 0 Series E. m. u.), Transactions of the Japan Society of Mechanical Engineers (in Japanese), Vol. 57, No. 539 (1991), DOI: 10.1299/kikaic.57.2211

Tanifuji, K., Yoshioka, H., and Miyashita, S: A prediction of riding comfort with an artificial generation of track irregularity, Transactions of the Japan Society of Mechanical Engineers (in Japanese), Vol. 56, No. 523 (1990), DOI: 10.1299/kikaic.56.574

Tanifuji, K., and Michitsuji, Y: A Method for Estimation of Railway Vehicle Running Stability and Its Application to the Design of Self-Steering Truck, Transactions of the Japan Society of Mechanical Engineers (in Japanese), Vol. 66, No. 641 (2000), DOI: 10.1299/kikaic.66.247

Tanifuji, K, Kikkou, S, Sakanoue, K., and Namba, K: Modelling of aerodynamic force acting in tunnel for analysis on riding comfort as a train, Transactions of the Japan Society of Mechanical Engineers (in Japanese), Vol. 72, No. 720 (2006), DOI: 10.1299/kikaic.72.2426

Toshimitsu, K., Tanifuji, K., and Soma, H: Potential of Improving Riding Comfort of High-Speed Trains with Inter-Lateral vehicle Damper, Transactions of the Japan Society of Mechanical Engineers (in Japanese), Vol. 73, No. 733 (2007), DOI: 10.1299/kikaic.73.2485